Biomedicine & Pharmacotherapy 155 (2022) 113736

Contents lists available at ScienceDirect

Biomedicine & Pharmacotherapy

journal homepage: www.elsevier.com/locate/biopha

Azulene hydrazide-hydrazones for selective targeting of pancreatic cancer cells

Tereza Brogyányi [a,b], Robert Kaplánek [a,c], Zdeněk Kejík [a,c], Božena Hosnedlová [a,c], Veronika Antonyová [a,c], Nikita Abramenko [a], Kateřina Veselá [a,c], Pavel Martásek [c], Martin Vokurka [b], Des R. Richardson [d], Milan Jakubek [a,c,*]

[a] BIOCEV, First Faculty of Medicine, Charles University, Prague, Průmyslová 595, 252 50 Vestec, Czech Republic
[b] Institute of Pathological Physiology, First Faculty of Medicine, Charles University and General University Hospital in Prague, U Nemocnice 5, 128 53 Prague, Czech Republic
[c] Department of Paediatrics and Inherited Metabolic Disorders, First Faculty of Medicine, Charles University and General University Hospital in Prague, Ke Karlovu 455, 120 00 Prague, Czech Republic
[d] Centre for Cancer Cell Biology and Drug Discovery, Griffith Institute for Drug Discovery, Griffith University, Nathan, Brisbane, QLD, Australia

ARTICLE INFO

Keywords:
Hydrazone
Cancer
Chelators
NDRG1
HIF-1α
TfR1

ABSTRACT

Dysregulation of iron homeostasis is one of the important processes in the development of many oncological diseases, such as pancreatic cancer. Targeting it with specific agents, such as an iron chelator, are promising therapeutic methods. In this study, we tested the cytotoxicity of novel azulene hydrazide-hydrazone-based chelators against pancreatic cancer cell lines (MIA PaCa-2, PANC-1, AsPC-1). All prepared chelators (compounds **4**-**6**) showed strong cytotoxicity against pancreatic cancer cell lines and high selectivity for cancer cell lines compared to the healthy line. Their cytotoxicity is lower than thiosemicarbazone-based chelators Dp44mT and DpC, but significantly higher than hydroxamic acid-based chelator DFO. The chelator tested showed mitochondrial and lysosomal co-localization and its mechanism of action was based on the induction of hypoxia-inducible factor-1-alpha (HIF-1α), N-myc downstream-regulated gene-1 (NDRG1) and transferrin receptor 1 (TfR1). This strongly implies that the cytotoxic effect of tested chelators could be associated with mitophagy induction. Lipinski's rule of five analyses was performed to determine whether the prepared compounds had properties ensuring their bioavailability. In addition, the drug-likeness and drug-score were calculated and discussed.

1. Introduction

Iron (Fe) is a crucial element necessary for many biological processes such as oxygen transport, energetic metabolism, detoxication of chemicals, and DNA synthesis [1,2]. Iron forms the core of heme, which is part of key cellular proteins such as cytochromes P450 and NO synthase, and this element is also present in non-heme structures (like ribonucleotide reductase necessary for DNA replication). Iron-sulfur clusters are other important iron-containing molecules present mainly in mitochondria [3].

On the other hand, the level of free iron must be tightly regulated because the excess of free divalent iron may participate in oxidative stress reaction resulting in the formation of free radicals (Fenton's chemistry), which may lead to cell and tissue damage [4]. Iron is also important for tumor cells (e.g., survival and division). The iron-related processes in carcinogenesis and tumor cell growth include cell metabolism, DNA replication, regulation of cell cycle, apoptosis, and ferroptosis. That makes iron a potential target for the treatment of especially those tumors that remain resistant to standard therapy [5]. So regulating iron levels with iron chelators is a promising way to treat these tumors [6].

Iron chelators are compounds that can bind tightly iron as well as other metals ions. These structures coordinate with intra- and extracellular iron and form complexes [7]. Especially oxygen, sulfur and nitrogen donor atoms within ligands are able to create a stable complex with iron. In human medicine, several effective chelators for removing iron have been developed and are in clinical use. Deferoxamine (DFOA, Desferal™), Deferasirox (Exjade™, Desifer™) and Deferiprone

* Corresponding author at: BIOCEV, First Faculty of Medicine, Charles University, Prague, Průmyslová 595, 252 50 Vestec, Czech Republic.
E-mail address: milan.jakubek@lf1.cuni.cz (M. Jakubek).

https://doi.org/10.1016/j.biopha.2022.113736
Received 1 July 2022; Received in revised form 19 September 2022; Accepted 20 September 2022
Available online 23 September 2022

(Ferriprox™) are used for iron overload therapy, e.g., in thalassemia and anaemia, both treated by repeated blood transfusions [8]. Other types of new chelators are under development and show promising results [9].

As mentioned above, chelators are a promising class of potential anticancer compounds [10]. Among them, hydrazones play an important role. Numerous peer-reviewed publications have shown that hydrazones can be effectively designed for selective function [11]. Thank to this, these relatively simple but potent compounds exhibit a wide range of biochemical and biological effects such as enzyme inhibition, DNA targeting, or ROS reduction [12]. In medical research, they are intensively studied for the treatment of microbial and viral infections, neurodegenerative disorders and especially oncological diseases [13–19]. At present, it is beginning to show that one of the very important effects of chelator application could be the induction of mitophagy [20]. It is well known that mitochondrial dysfunction is strongly associated with many human diseases such as neurodegenerative and oncological ones [21–24]. Damaged mitochondria produce reactive oxygen species, disrupt cellular metabolism and stimulate disease development. Elimination of dysfunctional mitochondria through mitophagy is a very important part of the protective mechanism and loss of mitochondrial function can significantly increase the risk of many serious diseases. However, the application of specific agents, such as mitophagy chelators, could be lead to the restoration of proper mitochondrial function and thus to the suppression of the above diseases [25]. This effect is thought to be related to the induction hypoxia-inducible factor-1-alpha (HIF-1α) signalling [26]. Decreased iron levels stimulate prolyl hydroxylase, which activates HIF-1α nuclear translocation [27]. One of the important HIF-1α dependent genes that could participate in HIF-1α control mitochondrial function is N-myc downstream-regulated gene-1 (*NDRG1*), its repression leads to mitochondrial fragmentation and loss of mitochondrial membrane potential [28]. In oncological diseases such as pancreatic cancer, expression can lead to a strong decrease in invasive capacity and spontaneous cancer cell metastases by inducing differentiation and reversing the metastatic phenotype.

This implies that *NDRG1* induction could be an important part of the mechanism of action of mitophagy chelators. According to the proposed model, Richardson et al. reported that intracellular iron levels regulate its expression and the iron chelator can be used as an inducer of *NDRG1* [29,30]. The effect of chelators on mitochondrial behavior and homeostasis should be considered much more.

The design of new chelators required building blocks with optimal lipophilicity, solubility, high electron density as well as suitable spectral properties for the fluorescence microscopy and analytical studies. Azulene, bicyclic non-benzenoid aromatic hydrocarbon, fulfil all above mentioned conditions [31]. Thus, we designed hydrazone-based chelators bearing azulene moiety. Variability of substitution pattern in hydrazone group (position and electron density characteristics of substituent) was used for finding optimal structure motive from the point of iron chelating ability and anticancer activity.

In this study, we present the original iron chelators, describe their basic properties, the principle of intracellular effects and the localization and mechanism of their action.

2. Materials and methods

2.1. Synthesis of chelators

2.1.1. Measurements and materials

All chemicals and solvents were purchased from commercial suppliers and used without further purification. NMR spectra were recorded on 300 MHz (^{1}H at 300 MHz, ^{13}C at 75 MHz) and 500 MHz (^{1}H at 500 MHz, ^{13}C at 126 MHz) instruments at room temperature in $CDCl_3$ and DMSO-*d6*. The chemical shifts (δ) are presented in ppm and coupling constants (J) are presented in Hz. The program MestReNova ver. 14.0.0 was used for processing the NMR spectra. Mass spectra were obtained using electrospray ionization (ESI) with triple quadrupole mass spectrometer TSQ Quantum Access and on LTQ Orbitrap spectrometer (HRMS).

2.1.2. Preparation of methyl 7-isopropyl-3-methylazulene-1-carboxylate (2)

5-Isopropyl-3-(methoxycarbonyl)− 2 H-cyclohepta[*b*]furan-2-one (1232 mg; 5 mmol) was dissolved in isopropanol (16 mL). Then propionaldehyde (1.1 mL; 15 mmol) was added followed by morpholine (1.35 mL; 15.3 mmol). The reaction mixture was stirred at 75 °C for 4 h (TLC petroleum ether/ethyl acetate 8:1 *v/v*). Then volatile compounds were removed under reduced pressure and the crude product was purified by column chromatography (silica gel; eluent petroleum ether/ethyl acetate 5:1 *v/v*). Methyl 7-isopropyl-3-methylazulene-1-carboxylate was obtained as a dark blue solid in the yield of 975 mg (80 %).

^{1}H NMR (300 MHz; $CDCl_3$): 1.41 (d, J = 6.9 Hz, 6 H, $C(CH_3)_2$); 2.58 (s, 3 H, CH_3); 3.20 (hept, J = 6.9 Hz, 1 H, $CH(CH_3)_2$); 3.94 (s, 3 H, OCH_3); 7.34 (m, 1 H); 7.69 (d, J = 10.2 Hz, 1 H, Azu-H); 8.16 (s, 1 H, Azu-H); 8.23 (dd, J = 9.8, 0.6 Hz, 1 H, Azu-H); 9.67 (d, J = 1.9 Hz, 1 H, Azu-H). ^{13}C NMR (75 MHz; $CDCl_3$): 12.6 (Azu-CH_3); 24.8 ((CH_3)$_2$); 39.2 (CH); 51.1 (OCH_3); 113.5 (C_{Azu}); 124.3 (C_{Azu}); 125.3 (CH_{Azu}); 133.6 (CH_{Azu}); 137.1 (CH_{Azu}); 137.8 (CH_{Azu}); 140.8 (CH_{Azu}); 141.2 (C_{Azu}); 141.6 (C_{Azu}); 148.2 (C_{Azu}); 166.1 (COO). Elem. Anal. Calcd for $C_{16}H_{18}O_2$: C, 79.31; H, 7.49. Found: C, 79.28; H, 7.54. ESI-MS (*m/z*): 243 $[M+H]^+$.

2.1.3. Preparation of 7-isopropyl-3-methylazulene-1-carbohydrazide (3)

Methyl 7-isopropyl-3-methylazulene-1-carboxylate (952 mg; 3.93 mmol) was dissolved in isopropanol (30 mL) and hydrazine hydrate (10 mL; 200 mmol) was added. The reaction mixture was stirred at 75 °C overnight. Then volatile compounds were removed under reduced pressure. The residue was purified by column chromatography (silica gel; eluent ethyl acetate). 7-isopropyl-3-methylazulene-1-carbohydrazide was obtained as a dark blue solid in the yield of 876 mg (92 %).

^{1}H NMR (300 MHz; $CDCl_3$): 1.39 (d, J = 6.9 Hz, 6 H, $C(CH_3)_2$); 2.57 (s, 3 H, CH_3); 3.18 (hept, J = 6.9 Hz, 1 H, $CH(CH_3)_2$); 4.20 (s, 2 H, NH_2); 7.29 (m, 1 H, Azu-H); 7.39 (s, 1 H, Azu-H); 7.67 (m, 1 H, Azu-H); 7.79 (s, 1 H, Azu-H); 8.21 (dd, J = 9.9, 1.0 Hz, 1 H, Azu-H); 9.66 (d, J = 1.9 Hz, 1 H, NH). ^{13}C NMR (75 MHz; $CDCl_3$): 12.6 (Azu-CH_3); 24.8 ((CH_3)$_2$); 39.1 (CH); 115.2 (C_{Azu}); 124.1 (C_{Azu}); 124.5 (CH_{Azu}); 133.8 (CH_{Azu}); 135.7 (CH_{Azu}); 137.8 (CH_{Azu}); 138.1 (CH_{Azu}); 140.0 (C_{Azu}); 140.3 (C_{Azu}); 147.3 (C_{Azu}); 167.7 (CONH). Elem. Anal. Calcd for $C_{15}H_{18}N_2O$: C, 74.35; H, 7.49; N, 11.56. Found: C, 74.31; H, 7.52. ESI-MS (*m/z*): 243 $[M+H]^+$.

2.1.4. Preparation of hydrazone 4

7-isopropyl-3-methylazulene-1-carbohydrazide (**3**; 46 mg; 0.19 mmol) and 2-hydroxy-3-methoxybenzaldehyde (31 mg; 0.20 mmol) were mixed with isopropanol (10 mL). The reaction mixture was then stirred at 75 °C for 2 days. Then volatile compounds were evaporated under reduced pressure and residue was suspended in diethyl ether/petroleum ether mixture (1:1 *v/v*; 30 mL). The solid material was filtered, washed with additional portions of diethyl ether/petroleum ether mixture (1:1 *v/v*; 3 ×20 mL) and dried at 50 °C under vacuum. *N*'-(2-Hydroxy-3-methoxybenzylidene)− 7-isopropyl-3-methylazulene-1-carbohydrazide (**4**) was obtained as green solid 60 mg (84 %).

^{1}H NMR (500 MHz; DMSO-*d6*): 1.35 (d, J = 6.8 Hz, 6 H, $C(CH_3)_2$); 2.61 (s, 3 H, CH_3); 3.17 (m, 1 H, $CH(CH_3)_2$); 3.83 (s, 3 H, OCH_3); 6.87 (m, 1 H, Ar-H); 7.03 (d, J = 8.1 Hz, 1 H, Ar-H); 7.11 (d, J = 7.8 Hz, 1 H, Ar-H); 7.44 (m, 1 H, Ar-H); 7.85 (d, J = 10.0 Hz, 1 H, Ar-H); 8.30 (s, 1 H, Ar-H); 8.40 (d, J = 9.7 Hz, 1 H, Ar-H); 8.60 (s, 1 H, Ar-H); 9.73 (s, 1 H, CH=N); 11.39 (s, 1 H, NH); 11.89 (s, 1 H, OH). ^{13}C NMR (126 MHz; DMSO-*d6*): 12.5 (Azu-CH_3); 24.7 ((CH_3)$_2$); 38.5 (CH); 56.1 (OCH_3); 113.8 (CH_{Ar}); 115.1 (C_{Ar}); 119.3 (C_{Ar}); 119.3 (CH_{Ar}); 121.4 (CH_{Ar}); 123.8 (C_{Ar}); 125.5 (CH_{Ar}); 134.5 (CH_{Ar}); 137.0 (CH_{Ar}); 137.6 (CH_{Ar}); 138.9 (CH_{Ar}); 140.4 (C_{Ar}); 146.7 (CH=N); 147.2 (C_{Ar}); 147.3 (C_{Ar}); 148.1 (C_{Ar}), 161.5 (CONH). Elem. Anal. Calcd for $C_{23}H_{24}N_2O_3$: C, 73.38;

H, 6.43; N, 7.44. Found: C, 73.40; H, 6.46; N, 7.41. HRMS (ESI)$^+$: Calcd. for $C_{23}H_{24}N_2NaO_3$ $[M + Na]^+$ 399.16846; Found 399.16830.

2.1.5. Preparation of hydrazone 5

7-isopropyl-3-methylazulene-1-carbohydrazide (**3**; 46 mg; 0.19 mmol) and 2-hydroxy-1-naphthaldehyde (35 mg; 0.20 mmol) were mixed with isopropanol (10 mL). The reaction mixture was then stirred at 75 °C for 2 days. Then volatile compounds were evaporated under reduced pressure and residue was suspended in diethyl ether/petroleum ether mixture (1:1 *v/v*; 30 mL). The solid material was filtered, washed with additional portions of diethyl ether / petroleum ether mixture (1:1 *v/v*; 3 ×20 mL) and dried at 50 °C under vacuum. *N*'-((2-Hydroxynaphthalen-1-yl)methylene)− 7-isopropyl-3-methylazulene-1-carbohydrazide (**5**) was obtained as green solid 64 mg (85 %).

^{1}H NMR (500 MHz; DMSO-*d6*): 1.36 (d, $J = 6.8$ Hz, 6 H, $C(CH_3)_2$); 2.66 (s, 3 H, CH_3); 3.19 (m, 1 H, $CH(CH_3)_2$); 7.26 (d, $J = 9.0$ Hz, 1 H, Ar-H); 7.44 (m, 2 H, Ar-H); 7.63 (m, 1 H, Ar-H); 7.90 (m, 3 H, Ar-H); 8.20 (d, $J = 8.4$ Hz, 1 H, Ar-H); 8.33 (s, 1 H, Ar-H); 8.42 (d, $J = 9.7$ Hz, 1 H, Ar-H); 9.49 (s, 1 H, Ar-H); 9.78 (s, 1 H, CH=N); 11.99 (s, 1 H, NH); 13.09 (s, 1 H, OH). ^{13}C NMR (126 MHz; DMSO-*d6*): 12.3 (Azu-CH_3); 24.5 ($(CH_3)_2$); 38.2 (CH); 108.8 (C_{Ar}); 114.8 (C_{Ar}); 119.0 (CH_{Ar}); 120.4 (CH_{Ar}); 123.4 (CH_{Ar}); 123.6 (C_{Ar}); 125.2 (CH_{Ar}); 127.6 (CH_{Ar}); 127.8 (C_{Ar}); 129.0 (CH_{Ar}); 131.5 (C_{Ar}); 132.1 (CH_{Ar}); 134.3 (CH_{Ar}); 136.9 (CH_{Ar}); 137.1 (CH_{Ar}); 138.7 (CH_{Ar}); 140.1 (C_{Ar}); 144.4 (CH=N); 146.9 (C_{Ar}); 157.7 (C_{Ar}); 161.1 (CONH). Elem. Anal. Calcd for $C_{26}H_{24}N_2O_2$: C, 78.76; H, 6.10; N, 7.07. Found: C, 78.73; H, 6.13; N, 7.03. HRMS (ESI)$^+$: Calcd. for $C_{26}H_{24}N_2NaO_2$ $[M + Na]^+$ 419.17355; Found 419.17279.

2.1.6. Preparation of hydrazone 6

7-isopropyl-3-methylazulene-1-carbohydrazide (**3**; 46 mg; 0.19 mmol) and 4-(diethylamino)− 2-hydroxybenzaldehyde (39 mg; 0.20 mmol) were mixed with isopropanol (10 mL). The reaction mixture was then stirred at 75 °C for 2 days. Then volatile compounds were evaporated under reduced pressure and residue was suspended in diethyl ether/petroleum ether mixture (1:1 *v/v*; 30 mL). The solid material was filtered, washed with additional portions of diethyl ether/petroleum ether mixture (1:1 *v/v*; 3 ×20 mL) and dried at 50 °C under vacuum. *N*'-(4-(Diethylamino)− 2-hydroxybenzylidene)− 7-isopropyl-3-methylazulene-1-carbohydrazide (**6**) was obtained as green solid 65 mg (82 %).

^{1}H NMR (500 MHz; DMSO-*d6*): 1.11 (t, $J = 7.0$ Hz, 6 H, $N(CH_2CH_3)$); 1.35 (d, $J = 6.8$ Hz, 6 H, $C(CH_3)_2$); 2.60 (s, 3 H, CH_3); 3.16 (m, 1 H, $CH(CH_3)_2$); 3.36 (q, $J = 7.0$ Hz, 4 H, $N(CH_2CH_3)$); 6.14 (s, 1 H, Ar-H); 6.26 (d, $J = 9.0$ Hz, 1 H, Ar-H); 7.17 (d, $J = 9.0$ Hz, 1 H, Ar-H); 7.40 (m, 1 H, Ar-H); 7.83 (d, $J = 10.6$ Hz, 1 H, Ar-H); 8.26 (s, 1 H, Ar-H); 8.38 (m, 2 H, Ar-H); 9.71 (s, 1 H, CH=N); 11.59 (s, 1 H, NH); 11.73 (s, 1 H, OH). ^{13}C NMR (126 MHz; DMSO-*d6*): 12.3 (Azu-CH_3); 12.6 ($N(CH_2CH_3)_2$); 24.5 ($(CH_3)_2$); 38.2 (CH); 43.8 ($N(CH_2CH_3)_2$); 97.6 (CH_{Ar}); 103.5 (CH_{Ar}); 106.8 (C_{Ar}); 115.5 (C_{Ar}); 123.3 (C_{Ar}); 124.7 (CH_{Ar}); 131.4 (CH_{Ar}); 134.0 (CH_{Ar}); 136.8 (CH_{Ar}); 137.2 (CH_{Ar}); 138.4 (CH_{Ar}); 139.7 (C_{Ar}); 146.3 (C_{Ar}); 148.0 (CH=N); 149.8 (CH_{Ar}); 159.6 (CONH). Elem. Anal. Calcd for $C_{26}H_{31}N_3O_2$: C, 74.79; H, 7.48; N, 10.06. Found: C, 74.74; H, 7.52; N, 10.01. HRMS (ESI)$^+$: Calcd. for $C_{26}H_{31}N_3NaO_2$ $[M + Na]^+$ 440.23140; Found 419.23084.

2.2. Iron chelation

2.2.1. Instrumentation

The affinity of fluorescent chelators to iron was assayed by UV–VIS spectroscopy (Cary 400, Varian). The UV-Vis spectra were measured from 300 to 600 nm, with 1-nm data spacing in a 1-cm quartz cell at a scan rate of 300 nm/s, measurement was done at room temperature (25 ± 2 °C) [32].

2.2.2. Method

Iron ions (II,III) in an aqueous medium (water/DMSO, 99:1, *v/v*) were prepared. There is a significant effect on the binding constants, which depends on solvent, so all the titrations were performed in the same medium. The affinity of fluorescent chelators to iron was assayed by UV–VIS spectroscopy. It showed significant interaction. We observed changes in the absorbance of the chelators at the spectral maximum after adding iron. The concentration of the chelators were 10 μM and the concentration of Fe(II,III) was in the range of 0–0.5 mM. Conditional constants (K_a) were calculated from the absorbance changes ΔA of chelators **4**-**6** at the spectral maximum of their complexes with Fe(II) by nonlinear regression analysis with the Letagrop Spefo 2005 software. The computational model for conditional constants (Ka) is described and discussed in detail elsewhere [32], in the same way, that was used to study the interactions of the organic hosts with metal ions in the aqueous medium [33–37]. The error of the measurement was expressed as three times the standard deviation between the measured data and calculated curve.

2.3. Frontier orbital energies and surface electrostatic potential maps

Chemical reactivity and optical spectra of compounds are characterized by their frontier orbitals. There are two types of frontier orbitals - the highest occupied molecular orbital (HOMO) and the lowest unoccupied molecular orbital (LUMO). Thus, HOMO and LUMO isodensity surfaces are presented below. The structures of HOMO and LUMO orbitals may be used in assessing interaction geometries. The HOMO and LUMO orbital isosurfaces were generated with an isodensity value of 0.02 a.u [35].

2.4. Cell cultures

AsPC-1 (Human pancreas adenocarcinoma ascites metastasis) were grown in RPMI 1640 medium supplemented with 2 mM glutamine, 10 % fetal bovine serum (FBS), 100 units/mL penicillin and 0.1 mg/mL streptomycin, MIA PaCa-2 (Human Caucasian pancreatic carcinoma) were grown in DMEM medium supplemented with 2 mM glutamine, 10 % FBS, 100 units/mL penicillin and 0.1 mg/mL streptomycin. PANC-1 (Human Caucasian pancreas) were grown in DMEM medium supplemented with 4 mM glutamine, 10 % FBS, 100 units/mL penicillin and 0.1 mg/mL streptomycin. BJh-TERT (human fibroblasts) were grown in conditioned DMEM low glucose medium, supplemented with 2 mM glutamine, 1 % NEAA, 10 % FBS, 100 units/mL penicillin and 0.1 mg/mL streptomycin [38]. Human pancreas carcinoma cells were purchased from the American Type Culture Collection (ATCC). The cells were incubated in a humidified incubator with 5 % CO_2 at 37 °C and were always grown to 80–90 % confluency. The FBS was provided from Biosera (Nuaille, France) as well as all synthetic cell culture media.

2.5. Cytotoxic effect (MTT assay)

Cell metabolic activity was estimated by using colorimetric assay MTT by measuring mitochondria oxidative activity. Thiazolyl blue (3-(4,5-dimathylthiazol-2-yl)− 2,5-diphenyltetrazolium bromide) was purchased from P-LAB. Cell viability after exposure cells with tested compounds was measured on reader Tecan Infinite® 200 PRO and the absorbance was read at 580 nm. The half-maximal inhibitory concentration (IC_{50}) was estimated on three pancreas cancer cell lines (MIA PaCa-2, PANC-1, AsPC-1) and compared with the effect on the human fibroblast cell line (BJh-TERT). Cells were seated in 96-well plates microplates at a diversity of 5×10^3 cells/well and were incubated for 24-hours at 37 °C, then cells were treated with different concentrations of tested compounds for 48-hours, each concentration in four replications. After treatment cells with tested compounds, the medium was removed and MTT solution was added. The microplates with cells were incubated for 2 h at 37 °C. The crystals formed in the cell were dissolved with DMSO. Then the viability was measured. The cell inhibitory concentration (IC) was calculated using the equation IC = (APMS well/mean Acontrol wells) / 100 %. The half-maximal inhibitory

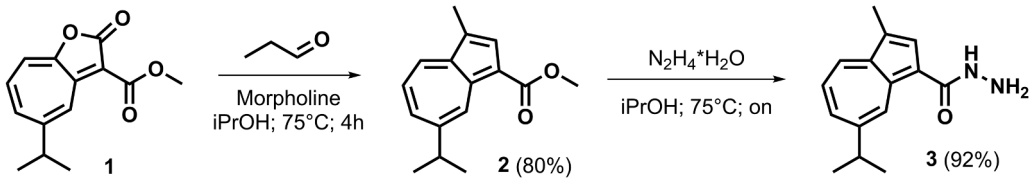

Scheme 1. Preparation of hydrazide **3**.

concentration (IC_{50}) was calculated from dose–response curves using GraphPad Prism software (v. 8.0.1, La Jolla, CA, USA).

2.6. In vitro imaging

2.6.1. Instrumentation

A fluorescence real-time microscopy study on live cells was performed on Leica TCS SP8 WLL SMD-FLIM microscope in the atmosphere with 5 % CO_2, at 37 °C. For visualization of cells was used a water objective HC PL APO CS2 63x (NA1,2) and three lasers with different excitation wavelengths: 1) 405 nm (10 % laser power), 2) 504 nm (8 % laser power), 3) 579 nm (8 % laser power), it was used HyD detectors (400 – 720 nm). Intracellular localization of chelators was compared with localizations of MitoTracker™ and LysoTracker™, provided from Thermo Fisher Scientific (Merck Life Science Ltd., Darmstadt, Germany).

2.6.2. Method

The intracellular localization was performed on living human fibroblasts (BJh-TERT) cells. The cells were cultivated in DMEM low glucose medium in atmosphere 5 % CO_2, at 37 °C. BJh-TERT were seeded in numbers of 5000 cells per well. The cells were left to adhere for at least 24 h in the incubator. After incubation, cells were washed two times with PBS. Then was added complete cell culture medium (DMEM l.g.) with chelators in the concentration of 1 μM, MitoTracker™ Red in the concentration of 50 nM and LysoTracker™ Green in the concentration of 300 nM. After adding the mixture, cells were incubated for 15 min (37 °C, 5% CO_2), intracellular uptake of the chelators was quite fast. After incubation, the cells were washed two times with PBS and a medium without phenol red was added.

2.7. Western blots

The changes in proteins (NDRG1, TfR1, HIF-1α) expression were studied on AsPC-1 tumor cell lines, after incubation with iron chelators. The investigation of the effect of iron chelators on protein expression was based on comparing our newly synthesized chelators with commercial iron chelates- di-2-pyridylketone-4-cyclohexyl-4-methyl-3-thiosemicarbazone (DpC), di-2-pyridylketone-4,4-dimethyl-3-thiosemicarbazone (Dp44mT) and desferrioxamine (DFO). The cells were treated with our chelators (**4**-**6**), DpC, Dp44mT in the concentration of 5 μM, with DFO in the concentration of 100 μM [39]. The AsPC-1 cell line was seeded in a number of 600,000 cells per well and was left to adhere at least for 24 h, till confluency was 70 %. It was used RPMI 1640 medium (20 % FBS, 1 % streptomycin). Subsequently, all medium was removed a and new medium containing tested chelator was added into wells. It was left incubated for 24 h. After 24 h cell lysis was done. From the cell lysate, increasing or decreasing effect on protein expression in comparison with control (cells without chelator) was determined. For tested proteins, there are three replications of experiments available to verify the result. The proteins expression changing was tested for three proteins (NDRG1, TfR1, HIF-1α), which are important for iron metabolism in cancer cell lines. TfR1 (transferrin receptor 1) is a protein involved in cellular iron uptake and in the regulation of cell growth. The expression of TfR1 is mainly regulated at the post-transcriptional level and its response to intracellular iron level. The NDRG1 is an iron-regulated metastasis suppressor protein. It is a protein involved mainly in cell growth, differentiation, DNA reparation and cell adhesion. The protein HIF-1α (hypoxia-inducible factor-1-alpha) is important in tumor angiogenesis. It is activated by low oxygen and by genetic events

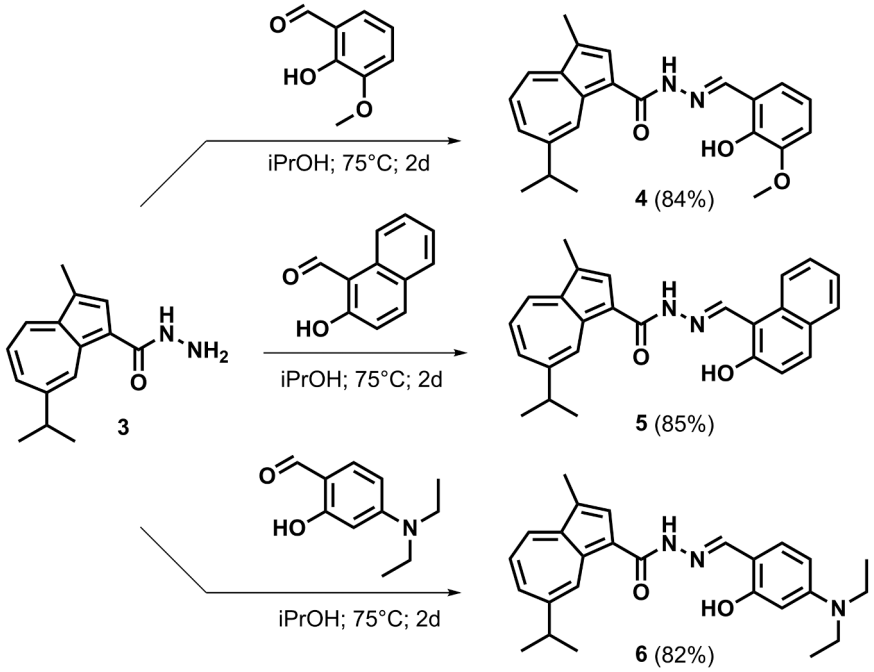

Scheme 2. Preparation of hydrazide-hydrazones **4**-**6**.

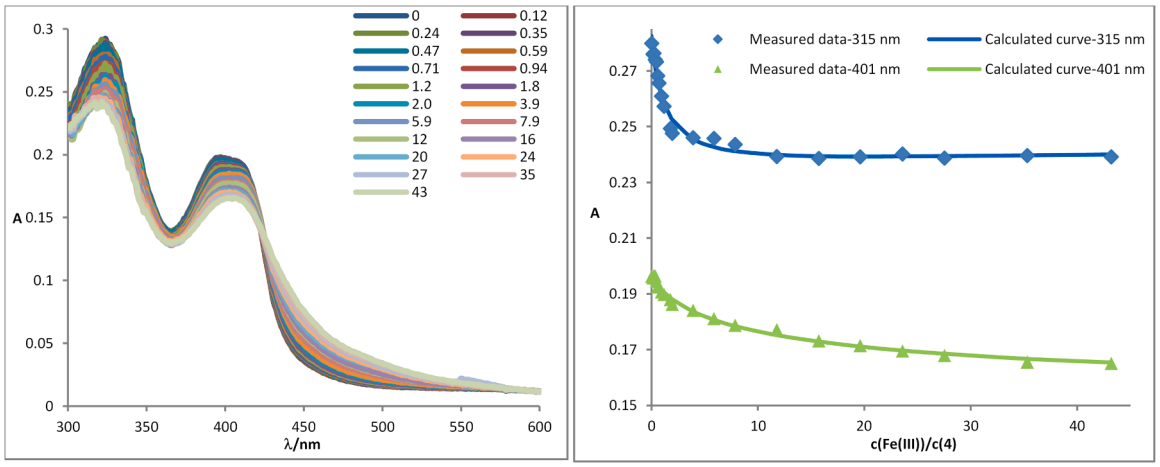

Fig. 1. UV-Vis of chelator **4** in the presence of Fe(III) ions (A) and titration curves (B) for chelator **4** (10 μM) showing the dependence of complex absorbance at 315 and 401 nm on Fe(III) concentration in the aqueous medium (water/DMSO, 99:1, *v/v*).

connected with tumor disease. Under hypoxia, HIF-1α becomes stable and acts as an important regulator of numerous hypoxia-inducible genes, which are related to angiogenesis, cell proliferation and glucose/iron metabolism.

3. Results and discussion

3.1. Synthesis

In our study, we synthesized new chelators based on hydrazide-hydrazones bearing azulene moiety. They were prepared by a three-step synthesis. In the first step, methyl 7-isopropyl-3-methylazulene-1-carboxylate (**2**) was prepared by the modified method according to Irvine and Majewski [40]. Thus, azulene moiety was prepared by the reaction of 5-isopropyl-3-(methoxycarbonyl)− 2 H-cyclohepta[*b*]furan-2-one (**1**) with propionaldehyde in the presence of morpholine in isopropanol at 75 °C in the yield of 80 % [14]. In the next step, methyl ester **2** was converted into corresponding carbohydrazide **3** by its reaction with the excess of hydrazine hydrate in isopropanol at 75 °C in the yield of 92 % (Scheme 1) [41].

In the last step, target hydrazide-hydrazones **4-6** were prepared by reaction of 7-isopropyl-3-methylazulene-1-carbohydrazide with 2-hydroxy-3-methoxybenzaldehyde, 2-hydroxy-1-naphthaldehyde or 4-(diethylamino)− 2-hydroxybenzaldehyde, respectively, in isopropanol at 75 °C in the yield of 82–85 % (Scheme 2).

NMR spectra of compound **2** showed signal for methyl-ester group as singlet at 3.94 ppm in ^{1}H NMR / 51.1 ppm in ^{13}C NMR, which disappeared after hydrazinolysis (not presented in compound **3**). After reaction with substituted 2-hydroxybenzaldehydes, signal for CH=N proton is clearly visible. It is known that hydrazones can exist as *E/Z* isomers at the C=N bond of the imino group due to geometric isomerism [42]. As a result, ^{1}H NMR shows splitting for the CH=N and NH protons. In the case of 2-hydroxybenzaldehyde hydrazide-hydrazones, *E*-isomer is preferred due to stabilization by a hydrogen bond between the phenolic hydroxyl group and enamine nitrogen [15]. In our case, ^{1}H NMR of hydrazide-hydrazones **4-6** has shown that both CH=N and NH protons are represented by only one singlet peak, indicating that they are formed exclusively as a single *E*-isomer (Fig. S6-S8). Signals of amide proton (NH) and phenolic hydroxy (OH) are presented as broad singlets (11.4–13.1 ppm).

3.2. Complexation studies

The association of chelators with iron ions (Fe(III) and Fe(II), respectively) was studied and we observed a significant interaction between chelators and iron ions. UV-Vis spectra of chelators in the presence of iron ions and titration curves for chelators showing the dependence of complex absorbance on the iron ion concentration in aqueous medium are shown in Figs. 1 and 2 (for compound **4**) and Figs. S1–S4 (Supplementary material; for compounds **5** and **6**). Conditional constants (K) were established for each chelator and determination of complex stoichiometry of chelators **4-6** was done. The results are

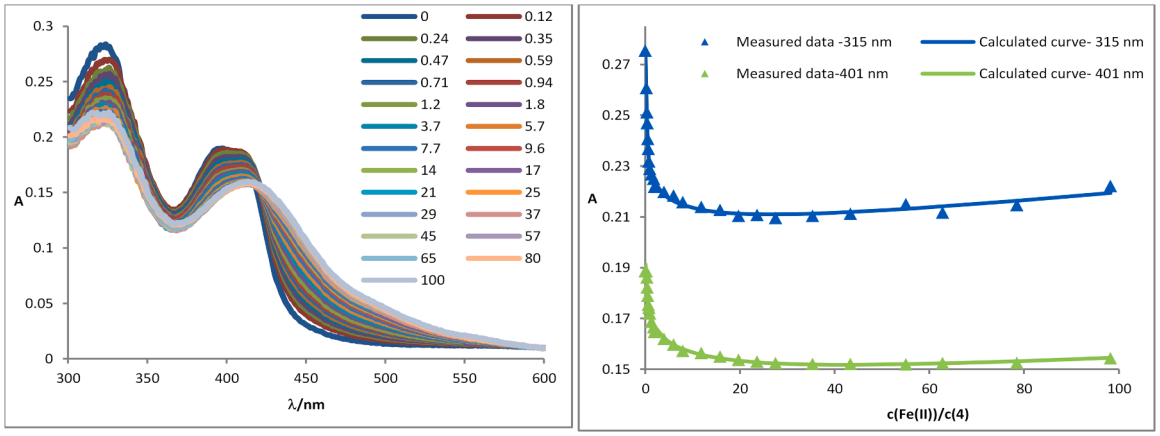

Fig. 2. UV-Vis of chelator **4** in the presence of Fe(II) ions (A) and titration curves (B) for chelator **4** (10 μM) showing the dependence of complex absorbance at 315 and 401 nm on Fe(II) concentration in the aqueous medium (water/DMSO, 99:1, *v/v*).

Table 1
Value of binding constants and complex stoichiometry of chelators **4-6** with iron ions.

Chelator	Fe (III)		Fe (II)	
	Log (K)	St[a]	Log (K)	St[a]
4	4.3 ± 0.42	1:1	5.5 ± 0.53	1:1
	9.5 ± 0.34	1:2	11.7 ± 0.65	1:2
5	4.7 ± 0.64	1:1	6.5 ± 0.19	1:1
	12.0 ± 0.89	1:2	14.8 ± 1.03	1:2
6	5.5 ± 0.41	1:1	7.9 ± 0.95	1:1
	9.5 ± 1.44	1:2	16.4 ± 0.25	1:2

[a] Stoichiometry (iron:chelator).

shown in Table 1.

In general, in the presence of iron ions, hydrazone chelators can form complexes 1:1, 1:2 (ion: chelator), or both. In accordance with this, we found both 1:1 and 1:2 complex stoichiometry for each chelator tested (**4-6**). Iron binding affinity values of chelators tested (**4-6**) (represented by the conditional constant K) showed significantly higher affinity toward Fe(II) ions (dominant cellular iron ion) compared to Fe(III) ions. This implies that their biological functions could be associated with the chelation of iron ions in cells. The highest binding affinity was found in chelator **6**.

3.3. Molecular modeling

The main objectives of the molecular modelling studies were to investigate metal binding ability of tested compounds. Molecular surface electrostatic potential maps are commonly used to describe electron distribution features in molecules. The simulation results showed that binding sites of chelators **4-6** are similar. Red-colored elements in the picture show more electronegative areas whereas blue-colored elements show more electropositive regions of the compound. The HOMO (highest-occupied molecular orbital) and LUMO (lowest-unoccupied molecular orbital) isosurfaces of compounds **4-6** are shown in Fig. 3. The highest-occupied molecular orbital (HOMO) and the lowest-unoccupied molecular orbital (LUMO) energies are − 10.0 and 5.84 eV for compound **4**, − 10.0 and 5.92 eV for compound **5**, − 5.74 and − 4.64 eV for compound **6**.

3.4. Cytotoxic activity

The cytotoxic effect of chelators **4-6** as anticancer agents was evaluated. We used MIA PaCa-2, PANC-1, AsPC-1 (pancreatic cancer cell lines) and BJh-TERT (human fibroblast cell line) to determine IC_{50} values. Cytotoxic activities are presented as IC_{50} values and they are summarized in Table 2 (IC_{50} values are expressed in μM concentrations), in Table S1 (Supplementary material; IC_{50} values are expressed in μg/mL concentrations) and shown in Fig. 4. Data were expressed as the average values of IC_{50} from ten independent experiments with SD ranging from 5 % to 50 % of the average values. Dose-response curves for compounds **4-6** are shown in Fig. S5 (Supplementary material).

The IC_{50} values for pancreatic cancer cell lines for the chelator **4** were in the range of 0.41–0.85 μM, for the chelator **5** from 0.67 to 3.55 μM, for the chelator **6** from 0.51 to 2.97 μM, respectively. The IC_{50} values for healthy cell line BJh-TERT were one order of magnitude

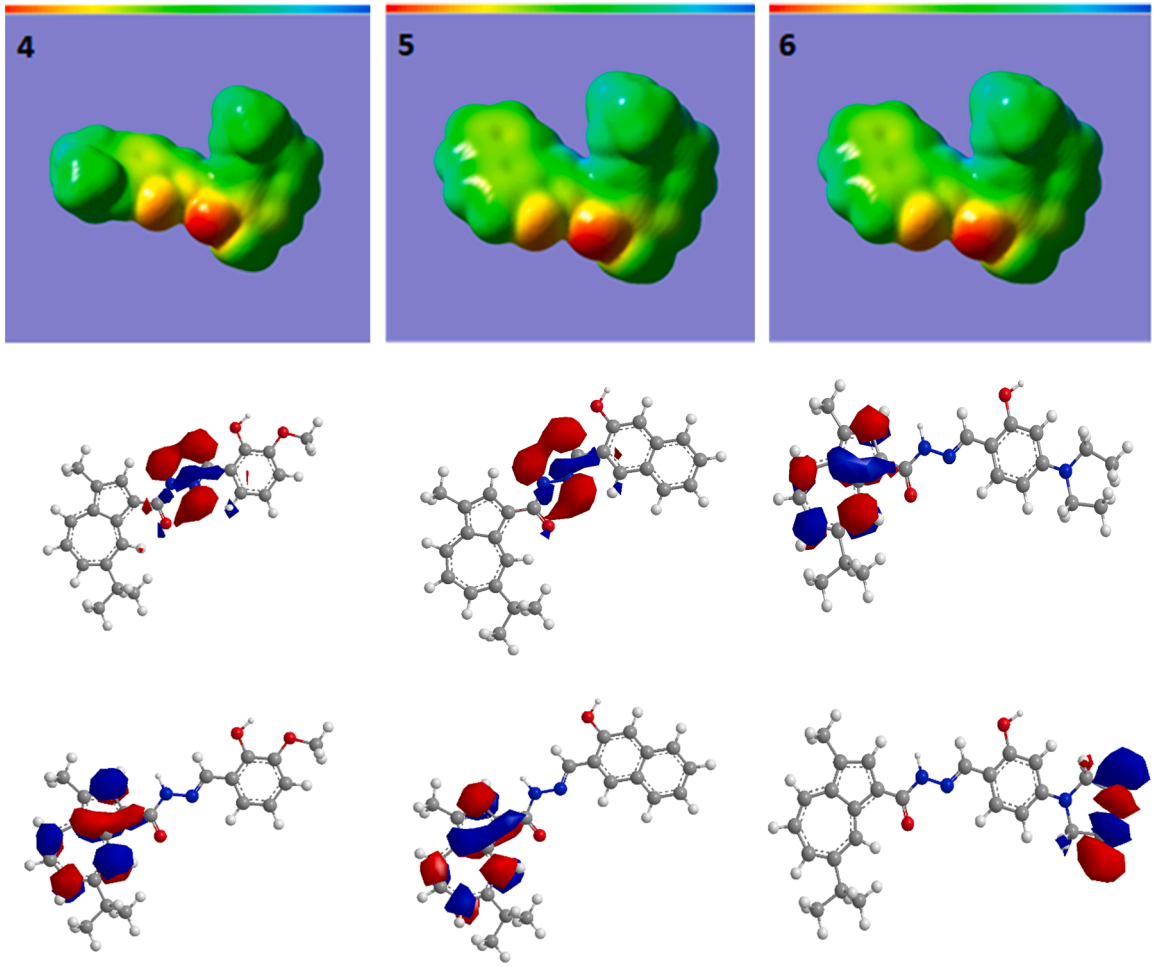

Fig. 3. Electrostatic potential, HOMO and LUMO maps of compounds **4-6**.

Table 2
Determined values of IC_{50} for chelators [μM] for different types of cell lines. * Data are presented as IC_{50} values ± c (three experiments).

Compound	IC_{50} [μM]			
	MIA PaCa-2	PANC-1	AsPC-1	BJh-TERT
4	0.41 ± 0.01	1.04 ± 0.06	0.77 ± 0.23	15.60 ± 0.19
5	1.71 ± 2.69	3.55 ± 2.12	2.97 ± 0.12	18.11 ± 1.41
6	0.85 ± 0.01	0.67 ± 2.30	0.51 ± 0.07	14.10 ± 0.21
DFO [45]	>200	>100	>200	N.D.
Dp44mT [43]	0.001 ± 0.001	0.004 ± 0.001	N.D.	N.D.
DpC [43]	0.005 ± 0.001	0.03 ± 0.002	N.D.	N.D.
5-Fluorouracil [43]	24.27 ± 6.35	62.30 ± 6.54	N.D.	N.D.

*IC_{50} values for **4-6** and DFO were determined after 24-h incubation, data for Dp44mT, DpC and 5-fluorouracil after 72-h incubation, respectively.

higher, in the range of 14.10–18.11 μM. We observed a slightly higher cytotoxic effect (lower IC_{50} values) on MIA PaCa-2 cells in comparison with PANC-1 and AsPC-1 cell lines, except for the compound **6**.

Comparison of biological activities of prepared derivatives **4-6** with those of other chelators against the same cell lines described in the literature is difficult due to various descriptors of activity and experimental conditions. Thiosemicarbazone-based chelators Dp44mT and DpC showed two- or three order of magnitude lower IC_{50} values (1–30 nM) for MIA PaCa-2 and PANC-1 cell lines. This high differences in activity were probably due to longer incubation time of Dp44mT and DpC [43,44]. Under the same condition, usually used anticancer agent 5-fluorouracil displayed one order of magnitude lower activity than **4-6**. Hydroxamic acid-based chelator DFO were not active (IC_{50} values > 100 μM) on all cell lines [43,44].

Comparison of biological activities of azulene hydrazide-hydrazones **4-6** with other hydrazone-based compounds described in the literature is difficult due to utilizing different cell lines, using various descriptors of activity (IC_{50}, EC_{50}, GI_{50}, etc.), as well as experimental conditions.

The selectivity indexes toward pancreatic cancer cells (Table 3) were calculated as a ratio of IC_{50} values for BJh-TERT-5 cell and IC_{50} values for the corresponding pancreatic cancer cell line (or the average IC_{50} value for all pancreatic cancer cell lines for the overall selectivity index). Thus, the selectivity index represents the selectivity for a specific pancreatic cancer cell line.

Compounds **4** and **6** showed great overall selectivity ($SI_{overall}$ = 21.1 and 20.8, respectively). It indicates the high potential of prepared compounds in the field of anticancer agents.

3.5. In vitro imaging

Tested compounds seem to be localized in mitochondria as well as in lysosomes. The localization data for BJh-TERT cells are shown in Figs. 5 and 6, the intracellular localization was examined by real-time live-cell fluorescent microscopy in human cell line BJh-TERT. The confirmation of localization was performed by calculating the Pearson correlation coefficient for lysosomes (Table 4) as a parameter of linear correlation of blue (chelators) and green (MTG) channel and for mitochondria (Table 5) as a parameter of linear correlation of blue (chelators) and red (MTR) channel. The calculated data showed a high correlation between their fluorescence emissions, meaning that they co-localized in both mitochondria and lysosomes. There can be several reasons. There is the possibility that chelators have dual selectivity and have a high affinity to mitochondria as well as to lysosomes at the same time. It is more likely that the chelators are localized in the lysosome which is related to mitophagy. It is known that loss of iron can impair mitochondrial function and it may cause mitophagy [46]. Mitochondria are highly dynamic endosymbiotic organelles that play key roles in cellular metabolism and apoptosis and iron chelation has a high effect on mitochondrial function. Mitophagy is mitochondrial macroautophagy and is described as selective autophagic degradation of mitochondria via lysosomes. It is mainly mediated by Parkin, PINK, AMBRA1, BNIP3, NIX, FUNDC. Decrase in the mitochondrial membrane potencial typical for the mitochondrial stress, or damage lead mitochondrial fusion with autophogosomes and its degragation [47,48]. The failure of this properly mechanism can appear and then develop oncogenic stresses that can stimulate or suppress tumorigenesis. It is known that iron chelation is a strong PINK1/Parkin-independent activator of mitophagy [48]. This fact can be responsible for the stimulation of cell death and be selective to cancer cells [49]. The link between iron chelators, intracellular iron levels and mitophagy was proved by transferrin receptor levels, which are increased in case of iron depletion. The correlation between mitophagy and transferrin receptor levels has been described and loss of free iron can cause mitophagy [48].

Table 3
Selectivity indexes (SI) toward pancreatic cancer cells for chelators **4-6**.

Compound	Selectivity index (SI)			
	MIA PaCa-2	PANC-1	AsPC-1	Overall
4	38.0	15.0	20.3	21.1
5	10.6	5.1	6.1	6.6
6	16.6	21.0	27.6	20.8

SI = [IC_{50} values for BJh-TERT]/[IC_{50} values for corresponding cancer cell line].

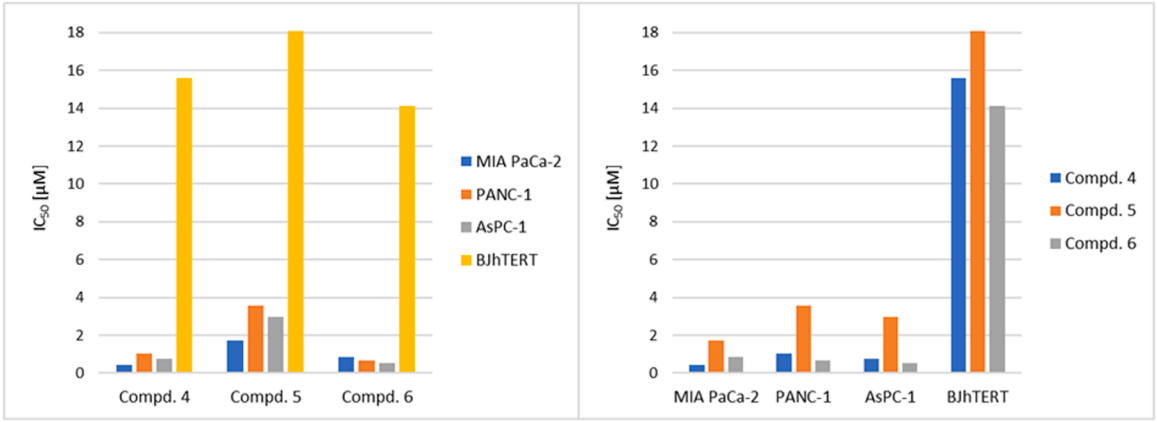

Fig. 4. IC_{50} values for chelators **4-6**. For statistical analysis, each treatment was compared with the untreated control.

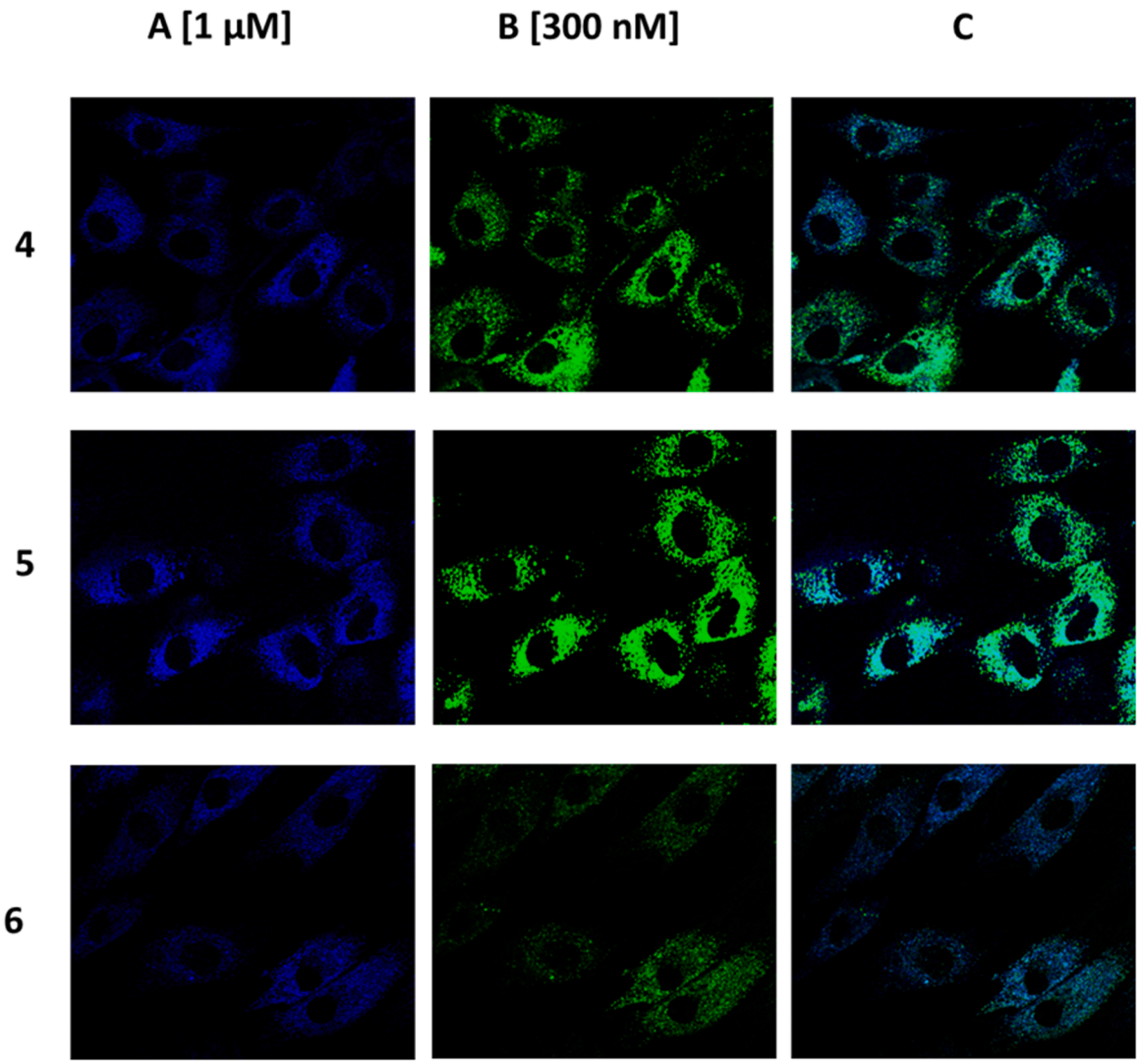

Fig. 5. Intracellular localization of the compounds (**4-6**) imaged in living BJh-TERT cells. **A:** chelator in the concentration of 1 μM; **B:** LysoTracker™ in the concentration of 300 nM; **C:** merge of images A,B.

3.6. Western blots

To understand the influence of compounds **4-6** on the iron homeostasis, three well-characterized iron chelators DFO, Dp44mT and Dpc were used to compare their effects on the Fe-dependent metabolic pathways.

In these studies, the cell line, namely AsPC-1, was incubated for 24 h with chelators DFO (100 μM), DP44mT (5 μM), DpC (5 μM) and the compounds **4-6** (5 μM). These concentrations were selected depending on the chelator's permeability and efficacy. Because DFO has a highly hydrophilic character and a very limited ability to permeate membranes, it was used at a higher concentration.

The results summarized above showed the ability of compounds **4–6** to chelate iron ions, their cytotoxic effect on tumor cell lines, and the ability to modify NDRG1, TfR1 and HIF-1α levels.

The well-known in vitro and in vivo studies showed that overexpression of NDRG1 significantly reduces the metastatic ability of cells. It was demonstrated that NDRG expression is regulated by cellular iron levels and induced by treatment with iron chelators. This means that these compounds **4-6** are potential anticancer agents, can prevent cell proliferation in cancer cell lines and lead to apoptosis [50]. Initial studies showed that iron chelators significantly increased the expression of NDRG1 relative to the control. The results showed higher expression of NDRG1 after treatment AsPC-1 cell line with compound **6**. It is clear that two bands for NDRG1 (≈ 46 kDa) appeared after treatment with compound Dp44mT and Dpc, but one NDRG1 (≈ 46 kDa) band was found for compounds DFO and compounds **4-6**. The appearance of these two NDRG1 bands is not very clear, there is the possibility that these two NDRG1 bands correspond to the phosphorylation states of the protein [51]. The effect of DFO, DpC, Dp44mT and compounds **4-6** to upregulate NDRG1 level was directly compared (Fig. 7 and Fig. S9). In cancer cells there are various alterations in the metabolism of iron; up-regulation of TfR1 expression at the cell surface is one of them. It is well known that the expression of TfR1 is regulated by the IRP-IRE mechanism, which depends on intracellular iron levels [52]. The down-regulation of TfR1 expression has a negative effect on cellular proliferation and leads to growth arrest and DNA damage [53]. On the other hand, the cytotoxic effects of some mitophagy chelators can be associated with their up-regulation [29,30]. The results showed upregulation of TfR1 after incubation cells with DFO, compounds **4–6** but increase in its expression was not so strong as up-regulation of NDRG1 after the same incubation time. The regulation of TfR1 by DpC and Dp44mT was not markedly increased when compared with the control as is demonstrated in Fig. 8 and Fig. S9.

It is well known that hypoxia occurs in tumorigenesis while tumors grow. Cancer cells response and adaptation to hypoxia are mediated by

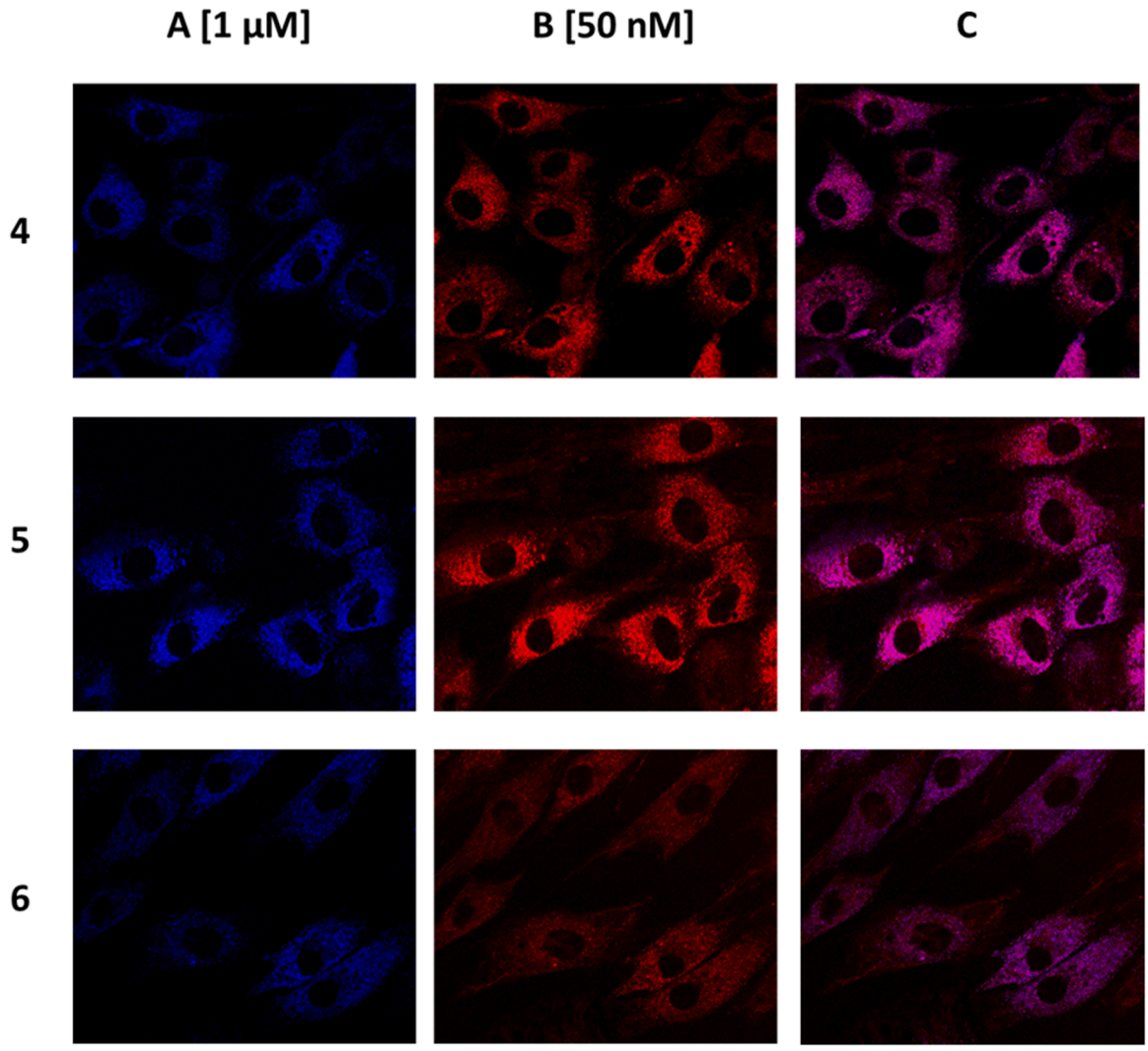

Fig. 6. Intracellular localization of the chelators (**4-6**) imaged in living BJh-TERT cells. **A:** Chelator in the concentration of 1 μM; **B:** MitoTracker™ in the concentration of 50 nM; **C:** merge of images A,B.

Table 4
Pearsońs correlation coefficient of **4-6** for lysosomes.

BJh-TERT cells	
Compound	Pearsońs correlation coefficient
4	0.84
5	0.81
6	0.60

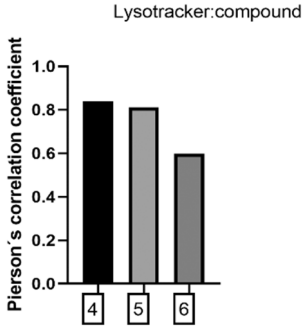

Table 5
Pearsońs correlation coefficient of **4-6** for mitochondria.

BJhTERT cells	
Compound	Pearsońs correlation coefficient
4	0.92
5	0.84
6	0.81

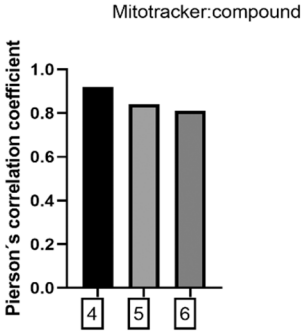

hypoxia-inducible factors (HIFs). HIFs are responsible for the regulation of proliferation, angiogenesis, inhibiting factors related to apoptosis, development of metastasis and many more [54]. Because hypoxia-inducible factor-1α plays a crucial role in the progression of pancreatic cancer, down-regulation of HIFs in cancer cells is a promising target for cancer therapy and improve its poor prognosis [55]. *In vitro* experiments showed several times lower expression of HIF-1α after incubation AsPC-1 with compounds 4 and 5 in comparison with DFO, Dp44mT and DpC. The inhibition is clearly visible in Fig. 9 and Fig. S10.

Details of statistical evaluation (measured values, SD, p-values,F-values, t-values, Chi-square values) for tested chelators are shown in Supplementary materials, Table S2.

Further research will be to control protein expression after different incubation times (6 h, 24 h) and to monitor the effect of chelators.

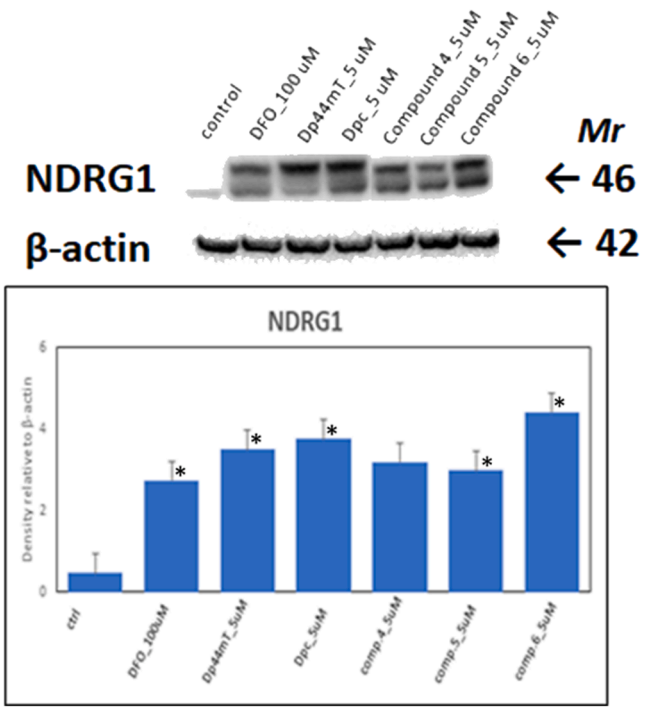

Fig. 7. The expression of NDRG1 in response to the treatment. * $p < 0.05$ vs. control, n = 4.

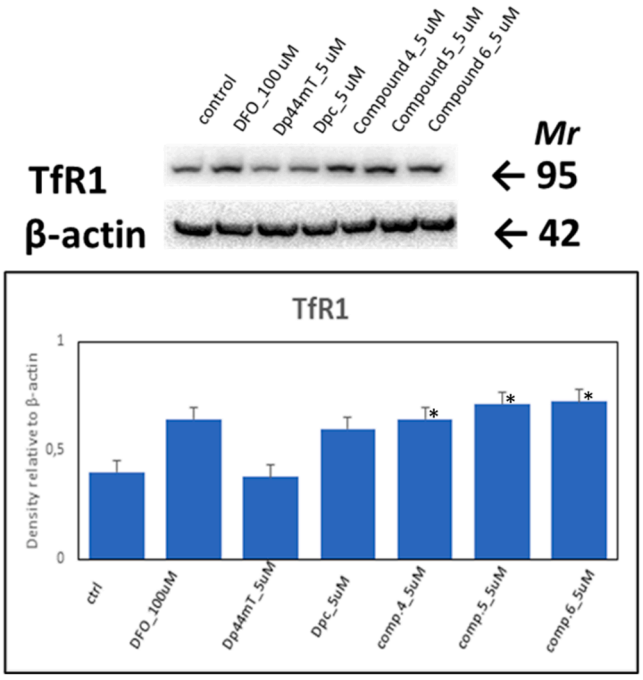

Fig. 8. The expression of TfR1 in response to the treatment. * $p < 0.05$ vs. control, n = 4.

3.7. Lipinski's rule of five analyses and drug-score factor

Lipinski's rule of five analyses was made to determine if prepared azulene hydrazide-hydrazones have properties that ensure their potential bioavailability. Lipinski's rule uses five criteria to determine if a substance is druglike. These criteria are as follows: ten or fewer hydrogen bond acceptors (HBA), five or fewer hydrogen bond donors (HBD), molecular weight under 500 Da, cLogP lower than 5. Tested drug

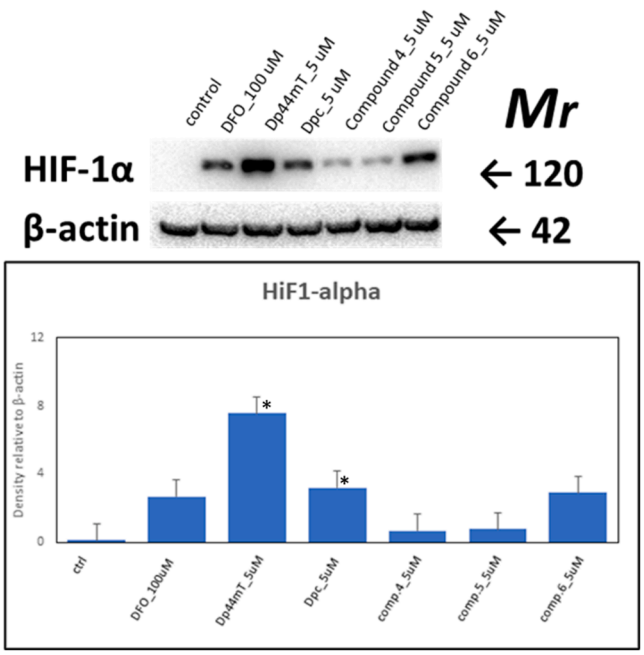

Fig. 9. The expression of HIF-1α in response to the treatment. * $p < 0.05$ vs. control, n = 4.

should be not more than one exception of the above rules [56]. The related criteria, Polar Surface Area (PSA) lower than 140 A^2, was also included in the analysis. The data is summarized in Table 6. All compounds meet Lipinski's rule of five. This suggests that compounds **4–6** may have good bioavailability. Compounds **5** and **6** have cLogP higher than 5, which means that this compound may not be able to penetrate the cell membrane due to high hydrophobicity. It should be mentioned that many classical anticancer drugs, such as doxorubicin, does not meet more than one of Lipinski's parameters and thus they display poor bioavailability. This problem can be solved using an appropriate formulation of the drug.

Moreover, drug-likeness and the drug-score factors were calculated for compounds **4-6** using Osiris® Property Explorer [56]. The drug-likeness score is a qualitative concept used in drug design for how a substance is drug-like with respect to Lipinski's rule of five parameters and substructural fragments contributions. A positive value states that compounds contain fragments that are frequently present in commercial drugs (about 80 % of the traded drugs have a positive drug-likeness value). The drug score combines drug-likeness factor, cLogP, logS, molecular weight, and toxicity risks. It allows predicting the overall potential of the compound as a drug. The drug-score of compounds **4-6** are shown in Table 6. Compounds **4-6** exhibited positive drug-likeness values and high drug-score values, which is comparable with the drug-score of commonly used anticancer drug - doxorubicin (drug-score 0.55).

Obtained score imply, that optimal azulene chelator structure motive is represent by compound **6**. It displayed better cytotoxicity for the tested cancer cell lines, except MIA PaCa-2, for which higher cytotoxicity have compound **4**. Nevertheless compounds **4** and **5** displayed higher value of Pearson's coefficient for mitochondrial and lysosomal localization. It could imply that compound **6** has not high potential for the mitophagy induction such as compounds **4** and **5**. Nevertheless, compound **6** display significantly higher increase in expression of NDRG1, TfR1 and HIF-1α in comparison to prepared compounds **4** and **5**. However, stimulation of their expression is marker of mitophagy activity [29,30]. It strongly suggests that biological effect of tested chelators, especially compound **6** is based in significant part on mitophagy induction. It could be explained by significantly higher binding affinity (represent by binding constants, Table 1) for Fe(II) ion

Table 6
Lipinski's rule of five parameters, drug-likeness and drug-score values for compounds **4-6**.

Compd.	H-bond acceptors	H-bond donors	Mw [Da]	cLogP	Polar surface area [A^2]	Drug- likeness	Drug-score
4	5	2	376.45	4.30	70.92	4.49	0.36
5	4	2	396.49	5.57	61.69	2.57	0.21
6	5	2	417.55	5.08	64.93	6.21	0.64

in comparison to compounds **4** and **5**.

4. Conclusions

In conclusion, we prepared three novel chelators based on substituted azulene carbohydrazide possessing 2-hydroxybenzylydene hydrazone moiety (**4-6**). Target compounds were prepared in three synthetic steps with high overall yields. All prepared chelators displayed a strong affinity for iron ions, mainly Fe(II). The anticancer activity of the prepared chelators was tested on three pancreatic cancer cell lines (MIA PaCa-2, PANC-1, AsPC-1) and the health cell line (human fibroblast BJh-TERT). They show potent cytotoxic activity for tested pancreatic cancer cell lines. Compounds **4** and **6** showed superior selectivity for all pancreatic cancer cell lines compared to the healthy cell line. In comparison with hydroxamic acid-based chelator DFO, **4-6** are more potent cytotoxic agents. On the other hand, thiosemicarbazone-based chelators Dp44mT and DpC showed significantly lower IC_{50} values for tested cancer cell lines (MIA PaCa-2 and PANC-1).

Observed phenomena were coupled with higher expression of NDRG1, HIF-1α and TfR1 and mitochondrial and lysosomal co-localization of tested chelators. This implies that the mechanism of their effect can be associated with mitophagy induction. All compounds meet Lipinski's rule of five. This suggests that compounds **4-6** should have good bioavailability. Compounds **4–6** exhibited relatively high drug-score values, which is comparable with the drug-score of classical anticancer drugs.

Taken together, our results demonstrate that azulene hydrazide-hydrazones bearing 2-hydroxybenzylydene moiety represent a promising structure motif in the design of potent anticancer agents with great selectivity against cancer cells and warrant further attention and preclinical development.

Funding

This work was supported by the project of Charles University in Prague (SVV260521; UNCE 204064) and the Ministry of Education, Youth, and Sports of Czech Republic, grant no. LM2018133 (EATRIS-CZ). This work was also supported by the Cooperation Program of Charles University. The research study was also funded by the Technology Agency of the Czech Republic within projects nos. TN01000013 and FW02020128. We also acknowledge the Operational Programme Research, Development, and Education within the project Center for Tumor Ecology - Research of the Cancer Microenvironment Supporting Cancer Growth and Spread (reg. no.CZ.02.1.01/0.0/0.0/16_019/0000785). We also thank the Ministry of Industry and Trade of Czech Republic for the financial support, grant no. FV40120. This work was also supported by the Ministry of Health of Czech Republic, grant nos. NU21-08-00407 and NU22-08-00160. We also thank the project National Institute for Cancer Research (Programme EXCELES, ID project no. LX22NPO5102) funded by the European Union - Next Generation EU. This work was also supported by the National Institute for Neurological Research (Programme EXCELES, ID Project No. LX22NPO5107) funded by the European Union - Next Generation EU.

CRediT authorship contribution statement

T. Brogyányi, B. Hosnedlová, V. Antonyová, N. Abramenko, K. Veselá: Investigation, Methodology, Validation, Writing – original draft. **R. Kaplánek, Z. Kejík:** Conceptualization, Investigation, Writing – original draft; **P. Martásek, M. Vokurka, D.R. Richardson:** Conceptualization, Resources, Supervision. **M. Jakubek:** Conceptualization, Resources, Visualization, Supervision, Writing – original draft. The publication has been approved by all of authors.

Conflict of interest statement

There are none.

Data availability

Data will be made available on request.

Acknowledgements

We acknowledge Imaging Methods Core Facility at BIOCEV, an institution supported by the MEYS CR (Large RI Project LM2018129 Czech-BioImaging) and ERDF (project No. CZ.02.1.01/0.0/0.0/16_013/0001775) for their support with obtaining imaging data presented in this paper.

Appendix A. Supporting information

Supplementary data associated with this article can be found in the online version at doi:10.1016/j.biopha.2022.113736.

References

[1] S. Puig, et al., The elemental role of iron in DNA synthesis and repair, Metallomics 9 (11) (2017) 1483–1500.
[2] T. Iyanagi, C. Xia, J.J. Kim, NADPH-cytochrome P450 oxidoreductase: prototypic member of the diflavin reductase family, Arch. Biochem Biophys. 528 (1) (2012) 72–89.
[3] M. Cardenas-Rodriguez, A. Chatzi, K. Tokatlidis, Iron-sulfur clusters: from metals through mitochondria biogenesis to disease, J. Biol. Inorg. Chem. 23 (4) (2018) 509–520.
[4] N. Bresgen, P.M. Eckl, Oxidative stress and the homeodynamics of iron metabolism, Biomolecules 5 (2) (2015) 808–847.
[5] M. El Hout, et al., A promising new approach to cancer therapy: targeting iron metabolism in cancer stem cells, Semin. Cancer Biol. 53 (2018) 125–138.
[6] K. Gaur, et al., Iron and copper intracellular chelation as an anticancer drug strategy, Inorganics 6 (4) (2018) 38.
[7] Y. Yu, et al., Iron chelators for the treatment of cancer, Curr. Med. Chem. 19 (17) (2012) 2689–2702.
[8] Chuang, T.Y., et al., Combined chelation with high-dose deferiprone and deferoxamine to improve survival and restore cardiac function effectively in patients with transfusion-dependent thalassemia presenting severe cardiac complications, Annals of Hematology, 6.
[9] M. Whitnall, et al., A class of iron chelators with a wide spectrum of potent antitumor activity that overcomes resistance to chemotherapeutics, Proc. Natl. Acad. Sci. USA 103 (40) (2006) 14901–14906.
[10] M. Jung, et al., Iron as a central player and promising target in cancer progression, Int. J. Mol. Sci. 20 (2) (2019) 18.
[11] D.B. Lovejoy, et al., PCTH: a novel orally active chelator for the treatment of iron overload disease, Hemoglobin 30 (1) (2006) 93–104.
[12] M. Fryknas, et al., Iron chelators target both proliferating and quiescent cancer cells, Sci. Rep. 6 (2016) 11.
[13] S. Rollas, S.G. Kucukguzel, Biological activities of hydrazone derivatives, Molecules 12 (8) (2007) 1910–1939.
[14] R. Kaplanek, et al., Synthesis and biological activity evaluation of hydrazone derivatives based on a Troger's base skeleton, Bioorg. Med. Chem. 23 (7) (2015) 1651–1659.
[15] R. Kaplanek, et al., Caffeine-hydrazones as anticancer agents with pronounced selectivity toward T-lymphoblastic leukaemia cells, Bioorg. Chem. 60 (2015) 19–29.

[16] L. Popiolek, Hydrazide-hydrazones as potential antimicrobial agents: overview of the literature since 2010, Med Chem. Res. 26 (2) (2017) 287–301.
[17] F.R. Pavan, et al., Thiosemicarbazones, semicarbazones, dithiocarbazates and hydrazide/hydrazones: anti-Mycobacterium tuberculosis activity and cytotoxicity, Eur. J. Med. Chem. 45 (5) (2010) 1898–1905.
[18] C.W. D'Acunto, et al., Metallomics for Alzheimer's disease treatment: use of new generation of chelators combining metal-cation binding and transport properties, Eur. J. Med. Chem. 150 (2018) 140–155.
[19] M. Jakubek, et al., Hydrazones as novel epigenetic modulators: correlation between TET 1 protein inhibition activity and their iron(II) binding ability, Bioorg. Chem. 88 (2019), 102809.
[20] N. Wilfinger, et al., Novel p53-dependent anticancer strategy by targeting iron signaling and BNIP3L-induced mitophagy, Oncotarget 7 (2) (2016) 1242–1261.
[21] V. Antonyová, et al., Role of mtDNA disturbances in the pathogenesis of Alzheimer's and Parkinson's disease, DNA Repair 91–92 (2020), 102871.
[22] J.L. Fialova, et al., Novel mitochondria-targeted drugs for cancer therapy, Mini Rev. Med. Chem. (2020).
[23] Y. Wang, et al., The role of mitochondrial dynamics and mitophagy in carcinogenesis, metastasis and therapy, Front. Cell Dev. Biol. 8 (2020) 413.
[24] Y. Xie, et al., Mitophagy in pancreatic cancer, Front. Oncol. 11 (2021), 616079.
[25] Z.L. Zhang, et al., Somatic and germline mutations in the tumor suppressor gene PARK2 impair PINK1/Parkin-mediated mitophagy in lung cancer cells, Acta Pharmacol. Sin. 41 (1) (2020) 93–100.
[26] S. Riis, J.B. Murray, R. O'Connor, IGF-1 signalling regulates mitochondria dynamics and turnover through a conserved GSK-3 beta-Nrf2-BNIP3 pathway, Cells 9 (1) (2020) 19.
[27] K.C. Park, et al., Pharmacological targeting and the diverse functions of the metastasis suppressor, NDRG1, in cancer, Free Radic. Biol. Med. 157 (2020) 154–175.
[28] D.D. Guo, K.F. Xie, X.J. Luo, Hypoxia-induced elevated NDRG1 mediates apoptosis through reprograming mitochondrial fission in HCC, Gene 741 (2020) 6.
[29] N.T.V. Le, D.R. Richardson, Iron chelators with high antiproliferative activity up-regulate the expression of a growth inhibitory and metastasis suppressor gene: a link between iron metabolism and proliferation, Blood 104 (9) (2004) 2967–2975.
[30] S. Sahni, et al., The metastasis suppressor, N-myc downstream-regulated gene 1 (NDRG1), inhibits stress-induced autophagy in cancer cells, J. Biol. Chem. 289 (14) (2014) 9692–9709.
[31] T.O. Leino, et al., The azulene scaffold from a medicinal chemist's perspective: physicochemical and in vitro parameters relevant for drug discovery, Eur. J. Med. Chem. 237 (2022), 114374.
[32] L.G. Sillen, High-speed computers as supplement to graphical methods.3. twist matrix methods for minimizing error-square sum in problems with many unknown constants, Acta Chem. Scand. 18 (5) (1964) 1085. -&.
[33] M. Jakubek, et al., Benzoisothiazole-1,1-dioxide-based synthetic receptor for zinc ion recognition in aqueous medium and its interaction with nucleic acids, Supramol. Chem. 31 (1) (2019) 19–27.
[34] M. Jakubek, et al., Perimidine-based synthetic receptors for determination of copper(II) in water solution, Supramol. Chem. 30 (3) (2018) 218–226.
[35] M. Jakubek, et al., Water soluble chromone Schiff base derivatives as fluorescence receptor for aluminium(III), Supramol. Chem. 29 (1) (2017) 1–7.
[36] N. Abramenko, et al., Spectroscopic study of in situ-formed metallocomplexes of proton pump inhibitors in water, Chem. Biol. Drug Des. 97 (2) (2021) 305–314.
[37] V. Antonyová, et al., Non-psychotropic cannabinoids as inhibitors of TET1 protein, Bioorg. Chem. 124 (2022), 105793.
[38] T. Alkasalias, et al., Inhibition of tumor cell proliferation and motility by fibroblasts is both contact and soluble factor dependent, Proc. Natl. Acad. Sci. USA 111 (48) (2014) 17188–17193.
[39] R.S. Moussa, Z. Kovacevic, D.R. Richardson, Differential targeting of the cyclin-dependent kinase inhibitor, p21(CIP1/WAF1), by chelators with anti-proliferative activity in a range of tumor cell-types, Oncotarget 6 (30) (2015) 29694–29711.
[40] N.M. Irvine, M. Majewski, Synthesis of 1,3-Dimethylazulene, Org. Prep. Proced. Int. 27 (5) (1995) 592–595.
[41] J. Xu, D.L. Wang, K. Imafuku, Microwave-Assisted synthesis and antifungal activity of 2,5-disubstituted-1,3,4-oxadiazoles containing azulene moiety, Synth. Commun. 39 (12) (2009) 2196–2204.
[42] S. Kumar, D. Kumar, Polystyrene-supported iodobenzene diacetate (PSIBD)-mediated synthesis of 1,2-diacylbenzenes from 2-hydroxyaryl aldehyde/ketone acylhydrazones, Synth. Commun. 38 (21) (2008) 3683–3699.
[43] Z. Kovacevic, et al., Novel thiosemicarbazone iron chelators induce up-regulation and phosphorylation of the metastasis suppressor, NDRG1: a new strategy for the treatment of pancreatic cancer, Mol. Pharmacol. (2011) p. mol.111.073627.
[44] L. Siqueira, et al., Multi-target compounds acting in cancer progression: Focus on thiosemicarbazone, thiazole and thiazolidinone analogues, Eur. J. Med. Chem. 170 (2019).
[45] H. Qin, et al., The effect of deferoxamine on the proliferation of pancreatic cancer cell lines: 289, Off. J. Am. Coll. Gastroenterol. ACG 109 (2014) S89.
[46] L. Al-Akra, et al., Tumor stressors induce two mechanisms of intracellular P-glycoprotein-mediated resistance that are overcome by lysosomal-targeted thiosemicarbazones, J. Biol. Chem. 293 (10) (2018) 3562–3587.
[47] K. Daskalakis, et al., Increased autophagy/mitophagy levels in primary tumours of patients with pancreatic neuroendocrine neoplasms, Endocrine 68 (2) (2020) 438–447.
[48] G.F.G. Allen, et al., Loss of iron triggers PINK1/Parkin-independent mitophagy, EMBO Rep. 14 (12) (2013) 1127–1135.
[49] A.V. Kulikov, et al., Mitophagy: link to cancer development and therapy, Biochem. Biophys. Res. Commun. 482 (3) (2017) 432–439.
[50] Z. Kovacevic, D.R. Richardson, The metastasis suppressor, Ndrg-1: a new ally in the fight against cancer, Carcinogenesis 27 (12) (2006) 2355–2366.
[51] T. Sugiki, et al., N-myc downregulated gene 1 is a phosphorylated protein in mast cells, Biol. Pharm. Bull. 27 (5) (2004) 624–627.
[52] T.R. Daniels, et al., The transferrin receptor part I: biology and targeting with cytotoxic antibodies for the treatment of cancer, Clin. Immunol. 121 (2) (2006) 144–158.
[53] K.A. O'Donnell, et al., Activation of transferrin receptor 1 by c-Myc enhances cellular proliferation and tumorigenesis, Mol. Cell. Biol. 26 (6) (2006) 2373–2386.
[54] T.G. Lu, et al., Up-regulation of hypoxia-inducible factor antisense as a novel approach to treat ovarian cancer, Theranostics 10 (15) (2020) 6959–6976.
[55] T.S. Zhao, et al., Inhibition of HIF-1 alpha by PX-478 enhances the anti-tumor effect of gemcitabine by inducing immunogenic cell death in pancreatic ductal adenocarcinoma, Oncotarget 6 (4) (2015) 2250–2262.
[56] ⟨http://www.openmolecules.org/propertyexplorer/applet.html⟩.